ARTICLES
https://doi.org/10.1038/s41567-022-01689-7

nature physics

Holographic dynamics simulations with a trapped-ion quantum computer

Eli Chertkov[1,2] ✉, Justin Bohnet[1], David Francois[1], John Gaebler[1], Dan Gresh[1], Aaron Hankin[1], Kenny Lee[1,5], David Hayes[1], Brian Neyenhuis[1], Russell Stutz[1], Andrew C. Potter[3,4] and Michael Foss-Feig[1]

Quantum computers promise to efficiently simulate quantum dynamics, a classically intractable task central to fields ranging from chemistry to high-energy physics. Yet, quantum computational advantage has only been demonstrated for artificial tasks such as random circuit sampling, and hardware limitations and noise have limited experiments to qualitative studies of small-scale systems. Quantum processors capable of high-fidelity measurements and qubit reuse enable a recently proposed holographic technique that employs quantum tensor-network states, a class of states that efficiently compress quantum data, to simulate the evolution of infinitely long, entangled initial states using a small number of qubits. Here we benchmark this holographic technique in a trapped-ion quantum processor using 11 qubits to simulate the dynamics of an infinite entangled state. We observe the hallmarks of quantum chaos and light-cone propagation of correlations, and find excellent quantitative agreement with theoretical predictions for the infinite-size limit of the implemented model with minimal post-processing or error mitigation. These results show that quantum tensor-network methods, paired with state-of-the-art quantum processor capabilities, offer a viable route to practical quantum computational advantage on problems of direct interest to science and technology in the near term.

Simulating the dynamics of interacting quantum systems is a foundational problem in quantum science, underlying the computation of electronic and optical characteristics of materials and microelectronic devices, prediction of chemical reaction kinetics, and even shedding light on the development of the early Universe. Early exploration of quantum dynamics has already yielded fundamental insights into the quantum underpinnings of thermodynamics and quantum chaos[1] (and their alternatives[2]), as well as uncovered striking classes of universal behaviour and critical phenomena in the structure of quantum many-body entanglement. Unfortunately, simulating quantum dynamics with classical computers is also a notoriously difficult problem, generically requiring resources scaling exponentially in either size or evolution time of the simulated system. By contrast, it has been known, for some time, that quantum computers can simulate quantum dynamics with resources (qubit number and circuit depth) scaling only polynomially[3]. For this reason, quantum dynamics simulation is widely regarded as a likely candidate for the first realization of practical quantum advantage[4].

Large-scale quantum simulations of simple models have been achieved in special-purpose quantum simulation platforms[5–7], but modelling realistic materials and processes will require universal, fully programmable quantum computers. At present, however, such computers have small quantum memories (qubit numbers); even as they surpass the scale of ~50 qubits necessary to provide a quantum advantage in principle, much larger systems will be needed to simulate systems of typical physical interest, such as complex molecules or bulk materials. Recently, a variety of quantum simulation algorithms based on quantum tensor-network methods have been developed[8–16] that afford substantial resource savings when simulating systems with less than maximal entanglement. Especially when combined with opportunistic mid-circuit measurements and reuse of qubits during a quantum computation[10], quantum tensor-network algorithms enable the simulation of systems with far more quantum degrees of freedom than can be directly mapped onto the qubits available in hardware. When implemented on quantum computers with enough qubits to prohibit classical simulation, such algorithms may open an immediate path to quantum advantage in large-scale simulations of complex chemicals and materials.

In this work, we use Quantinuum's H1-1 and H1-2 trapped-ion quantum processors (some data in this paper were taken when model H1 quantum computers were operated by Honeywell Quantum Solutions) to implement the first experimental demonstration of the tensor-network-inspired holographic quantum dynamics simulation (holoQUADS) algorithm[10], which we use to simulate an initially entangled infinite-size spin system evolving under chaotic quantum dynamics. Our results demonstrate that the fidelities and mid-circuit measurements and qubit-reuse capabilities of the Quantinuum devices enable quantum tensor-network methods to perform accurate quantum dynamics simulations of large-scale many-body systems.

With conventional Hamiltonian simulation techniques, simulating the dynamics of a system of size L requires $O(L)$ qubits, and the achievable simulation time t is limited by gate fidelities. By interchanging resource scaling involving space (qubit number) and time (circuit depth), holoQUADS enables the time evolution of arbitrarily large systems up to time t set by the number of available qubits, independent of L, thereby allowing for the study

[1]Quantinuum, Broomfield, CO, USA. [2]Institute for Condensed Matter Theory and IQUIST and Department of Physics, University of Illinois at Urbana-Champaign, Urbana, IL, USA. [3]Department of Physics, University of Texas at Austin, Austin, TX, USA. [4]Department of Physics and Astronomy, and Stewart Blusson Quantum Matter Institute, University of British Columbia, Vancouver, British Columbia, Canada. [5]Present address: Google Research, Mountain View, CA, USA. ✉e-mail: eli.chertkov@quantinuum.com

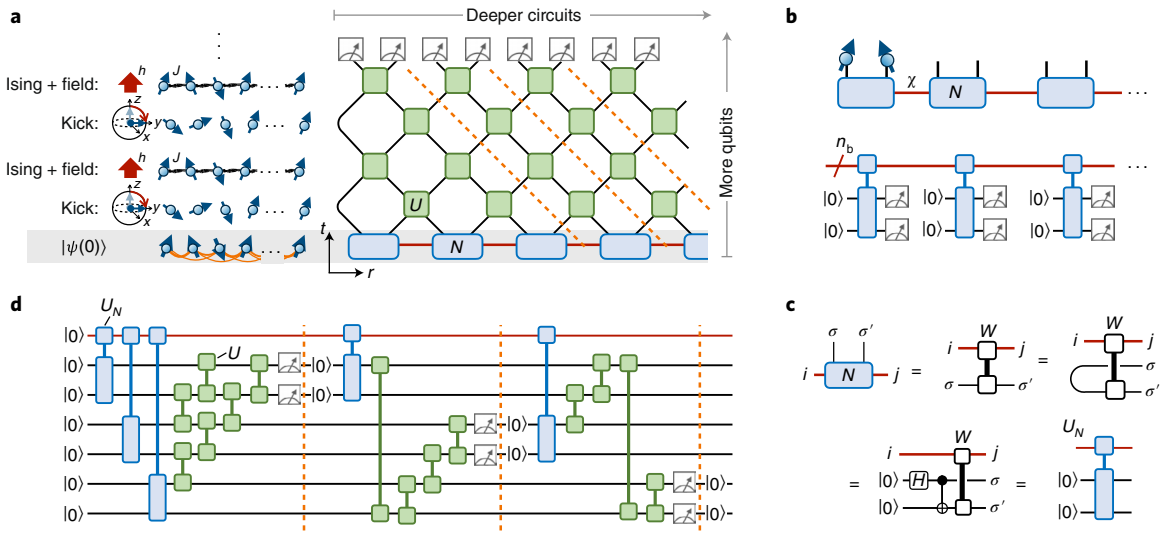

Fig. 1 | Holographic simulation of the kicked Ising model. a, Schematic of the SDKI model evolution ($t=2$ Floquet periods) and its quantum circuit implementation ($t=4$), which stroboscopically alternates between Ising interactions plus z field and $\pi/2$ 'kicks' by a transverse (x-axis) field. The green squares are dual-unitary gates, and the blue rectangles represent site tensors for the initial correlated MPS, $|\psi_0\rangle$. **b**, $|\psi_0\rangle$ is holographically prepared as a qMPS implemented by unitary gates (shown in detail in **c**) and mid-circuit measurements and resets (here qMPS measurements are shown in the σ^z basis). For holoQUADS, measurements are postponed until after the time evolution (as shown in **a**). **d**, The same state preparation and time evolution redrawn as a holographic quantum circuit using mid-circuit measurements and qubit recycling (holoQUADS algorithm).

of large systems approaching the 'thermodynamic' limit ($L\to\infty$) of interest to physicists. Moreover, holoQUADS leverages a compact representation of dynamics starting from initial correlated states, such as low-energy states of many-body Hamiltonians, requiring only (roughly) one additional qubit per unit of bipartite entanglement in the initial state. These initial correlated states can be analytically determined, through classical simulation, or using existing quantum algorithms, for example, quantum variational algorithms[17].

Taken together, these features ensure that qubit resources are not only much lower than with conventional methods but also are optimally utilized: time evolution of a state with initial entanglement entropy S_0 generically produces entanglement bounded by $S(t)\lesssim S_0+ct$ (c is a model-dependent constant)[18]. Since holoQUADS requires one qubit per bit of initial entanglement plus an additional number of qubits linear in t to enact the time evolution, resulting in a total qubit scaling $N\sim S(t)$, we see that every qubit is allocated directly towards the classically hard feature of time evolution in many-body quantum systems: the growth of entanglement.

HoloQUADS algorithm. HoloQUADS[10] simulates the time evolution of correlated initial states expressed as matrix product states (MPSs). For this work, we consider MPS of a half-infinite system with translationally invariant tensors over a two-site unit cell, which can be written as

$$|\psi_0\rangle=\sum_{\sigma_1,\sigma_2,\cdots\in\{\uparrow,\downarrow\}}\ell^{\mathrm{T}}\mathcal{N}^{(\sigma_1,\sigma_2)}\mathcal{N}^{(\sigma_3,\sigma_4)}\cdots|\sigma_1\sigma_2\sigma_3\sigma_4\cdots\rangle\,. \quad (1)$$

Here $|\sigma_1\sigma_2\ldots\rangle$ is the eigenstate of all Pauli operators σ_i^z with eigenvalues σ_i; $\mathcal{N}$ are rank-four tensors, that is, $\chi\times\chi$ matrices for each spin configuration (σ_i,σ_{i+1}); ℓ is a vector specifying the left-boundary condition; and bond dimension χ controls the amount of entanglement present in the state (very roughly, to capture a state with bipartite entanglement S, one needs $\chi\approx e^S$). As originally discussed elsewhere[19], any MPS can be realized as a quantum circuit where tensors $\mathcal{N}$ are implemented by a unitary $U_{\mathcal{N}}$ acting on a pair of 'system' qubits (representing a pair of neighbouring spins) initialized to $|0\rangle$, and $n_b=\lceil\log_2\chi\rceil$ 'bond' qubits that represent the χ-dimensional bond space. Following the language used elsewhere[12], we refer to MPS prepared this way on a quantum processor as quantum MPS (qMPS).

Although a length-$2L$ section of the half-infinite qMPS described above naively requires n_b+2L qubits to represent, mid-circuit measurements and qubit reuse allows us to 'holographically' represent it using only n_b+2 qubits[10,20] (Fig. 1b). An MPS evolving in time under the influence of a one-dimensional (1D) quantum circuit with layers of gates acting on neighbouring qubits also admits a holographic representation (Fig. 1). Due to the causal 'light-cone' structure of the quantum circuit and the qMPS initial state, the measurement results at the top (larger t) of the circuit are only affected by a subset of qubits at the bottom (smaller t). The circuit can, therefore, be executed going from left to right in slices bounded by the orange dashed lines shown in Fig. 1a,d, where in each slice, two qubits are reset for later reuse. Simulating t layers of nearest-neighbour time evolution of the MPS with bond dimension χ (equation (1)) with holoQUADS requires n_b+t+2 qubits ($n_b=\lceil\log_2\chi\rceil$), giving a logarithmic resource reduction compared with classical tensor-network techniques (which require memory scaling polynomially with χ and exponentially in t). Note that the scaling is independent of L; therefore, holoQUADS can be used to time evolve an arbitrarily large section of a half-infinite qMPS. Moreover, the size-$2L$ subsystem simulated by holoQUADS can span multiple depth-t light cones of width $2t+1$, which allows for the measurement of correlation functions separated by distances $r>2t+1$ (which can be non-zero due to the correlations present in the initial qMPS state).

Chaotic circuit dynamics benchmark. As the first demonstration of holoQUADS, we focus on the dynamics of the self-dual kicked Ising (SDKI) model[21,22]. In this model, a spin chain evolves under an Ising interaction and integrability-breaking longitudinal field h and is periodically 'kicked' by a transverse (X) field:

$$H(t)=\sum_i\left(\frac{\pi}{4}\sigma_i^z\sigma_{i+1}^z+h\sigma_i^z+\frac{\pi}{4}\sum_{n\in\mathbb{Z}}\delta(t-n)\sigma_i^x\right). \quad (2)$$

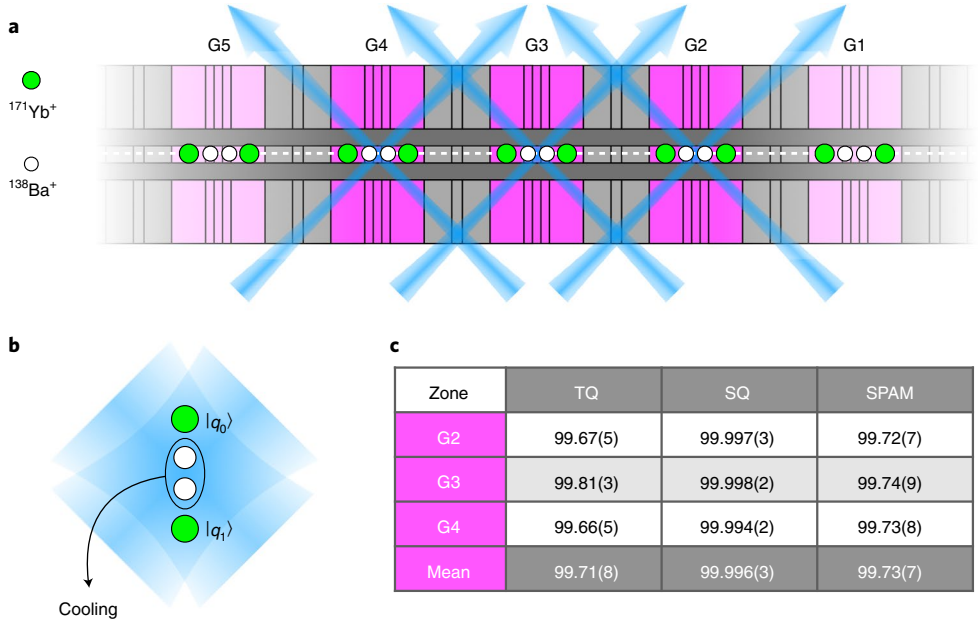

c

Zone	TQ	SQ	SPAM
G2	99.67(5)	99.997(3)	99.72(7)
G3	99.81(3)	99.998(2)	99.74(9)
G4	99.66(5)	99.994(2)	99.73(8)
Mean	99.71(8)	99.996(3)	99.73(7)

Fig. 2 | Quantum computer used in this work. a, Section of the Quantinuum H1-1 segmented-electrode surface trap, showing five gate zones in purple (750-μm-wide ion-crystal extents and laser-beam waists are not drawn to scale). The computer operates similar to the one described elsewhere[35] (except with the parallel-gate operation across the three central gate zones (G2–G4)), with $^{171}Yb^+$ qubit ions (green) and $^{138}Ba^+$ coolant ions (white) stored in either two-ion or four-ion crystals. Arbitrary pairing of qubits is achieved by transporting ions[36–38] along the linear radio-frequency null (dashed line) 70 μm above the surface. **b**, Sympathetic ground-state cooling followed by our two-qubit, phase-insensitive Mølmer–Sørenson gate is implemented in parallel across G2–G4 on Yb–Ba–Ba–Yb crystal configurations. Each crystal is roughly 8 μm in extent, and the cooling and gate lasers (wavelengths, 493 and 368 nm, respectively) have nominal beam waists of 17.5 μm. **c**, Typical (that is, representative over the duration of data taking) average fidelities of single-qubit (SQ) gates, two-qubit (TQ) gates and combined state preparation and measurement (SPAM) undertaken via randomized benchmarking.

Here $\boldsymbol{\sigma}_i$ are Pauli operators on site i of length-$2L$ spin chain. For $h \neq 0$, the SDKI is non-integrable[23], exhibiting the chaotic and thermalizing behaviour generically expected for non-integrable quantum dynamics. Moreover, recent analytical techniques enable the exact calculations of many of its properties[22–24], rendering it a powerful benchmark for the performance of holoQUADS.

As illustrated in Fig. 1a, the time-evolution operator of the SDKI model, namely, $\mathcal{U}_t = \mathcal{T}\{e^{-i\int_0^t H(s)ds}\}$, can be recast (at discrete times $t \in \mathbb{Z}$ and up to boundary terms in time) as a 1D quantum circuit consisting of alternating even–odd layers of two-qubit gates as[23,24]

$$U = (u_+ \otimes u_-)e^{-i\frac{\pi}{4}(\sigma^x\otimes\sigma^x+\sigma^y\otimes\sigma^y)}(v_- \otimes v_+). \quad (3)$$

Here $u_+ = e^{-i\sigma^z}e^{i\frac{\pi}{4}\sigma^x}e^{-i\frac{\pi}{4}\sigma^y}, u_- = e^{i\frac{\pi}{4}\sigma^x}e^{-i\frac{\pi}{4}\sigma^y}, v_- = e^{i\frac{\pi}{4}\sigma^y}e^{-ih\sigma^z}$ and $v_+ = e^{i\frac{\pi}{4}\sigma^y}$ are single-qubit rotations. For any single-qubit unitaries $u_\pm, v_\pm$, this gate satisfies a special dual-unitary property[23,24]: $U^\dagger U = \mathbb{1} = \tilde{U}^\dagger\tilde{U}$, where the dual $\tilde{U}$ of a two-qubit gate U is defined by a reshuffling of indices, namely, $\langle k|\otimes\langle l|\tilde{U}|i\rangle\otimes|j\rangle = \langle j|\otimes\langle l|U|i\rangle\otimes|k\rangle$.

Dual-unitary circuits can be interpreted as circuits that generate time evolution in both time and space. Many of their properties, such as spectral form factors and entanglement spectra, spread of local operator correlations, and out-of-time ordered correlators, can be analytically computed for special initial conditions: either infinite-temperature states[23] or 'exactly solvable' MPSs[25] of the form shown in equation (1) with

$$\mathcal{N}_{i,j}^{(\sigma,\sigma')} = \langle j|\otimes\langle\sigma'|W|i\rangle\otimes|\sigma\rangle \quad (4)$$

defined by a generic unitary matrix $W \in U(2\chi)$. Although the dual-unitary property is clearly fine-tuned and results in some peculiar features that do not survive generic perturbations, such as correlations spreading at the maximum possible velocity, dual-unitary circuits (for example, for $h \neq 0$ in the SDKI model) are typically non-integrable and exhibit generic features of chaos, ergodicity and thermalization[26,27]. This combination of striking features and solvability make the SDKI model an important minimal model of quantum dynamics and, for our purposes, a useful benchmark for dynamical simulation. Another study[25] derived the exact thermodynamic-limit expressions for equal-time two-point correlation functions of Pauli operators. Following that work, we consider the smoothed correlation functions

$$C^{\alpha\beta}(r,t) = \frac{1}{4L}\sum_{j=1}^{2L}\sum_{\delta=0,1}\langle\psi_t|\sigma_j^\alpha\sigma_{j+r+\delta}^\beta|\psi_t\rangle, \quad (5)$$

for which the sum over δ removes the even–odd effect, making the correlations easier to visually interpret. Here $|\psi_t\rangle$ is the wavefunction after the tth layer of the circuit (Fig. 1a).

Implementation on a trapped-ion quantum processor. We implement holoQUADS of the SDKI model for a section with $2L = 32$ sites of a half-infinite chain on Quantinuum's H1-1 trapped-ion quantum processor (Fig. 2), using between three and eleven $^{171}Yb^+$ hyperfine qubits, depending on the number of simulated circuit layers (Table 1). Note that there is no strict limitation on L, since holoQUADS (as implemented here) simulates a half-infinite chain, and larger L would simply have incurred marginally longer run times on the quantum computer (scaling linearly with L). However, correlations outside the 32-site measurement window are negligible for the initial correlation length and evolution time accessible with currently available qubit numbers. Note that Table 1 shows the resources required for our holoQUADS experiments after a circuit identity was used to reduce the number of two-qubit gates (Supplementary Information).

Table 1 | Experimental resources

	$t=0$	$t=1$	$t=2$	$t=3$	$t=4$	$t=5$	$t=6$	$t=7$	$t=8$
No. of qubits	3	5	5	7	7	9	9	11	11
No. of SQ gates	214	273	308	360	394	454	488	556	590
No. of TQ gates	66	87	104	129	146	175	192	225	242
% leaked	3.1	1.7	2.0	1.9	2.4	3.6	3.7	1.7	2.5

The required resources and detected leakage for the nine dual-unitary holoQUADS experiments. Each column corresponds to the simulated time evolution of a half-infinite MPS for time t. For each value of t, the associated circuit extracts correlation functions over 32 lattice sites, which involved 32 mid-circuit measurements and qubit resets, and each circuit was repeated 1,000 times to gather statistics. The first row lists how many qubits were used in each experiment. The second and third rows list how many single-qubit (SQ) and native two-qubit (TQ) gates were used, respectively. The last row indicates the percentage of the 1,000 experimental trials that were discarded due to the detected leakage of bond qubits (Supplementary Information).

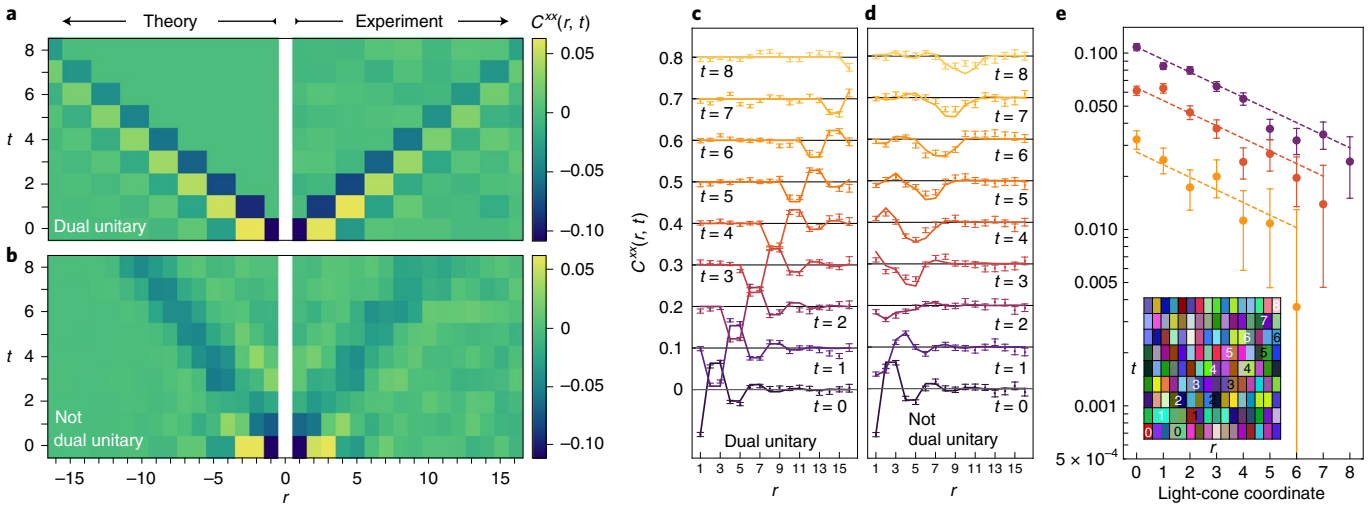

Fig. 3 | Experimental data. a, Colour plot of equal-time spin–spin correlators $C^{xx}(r,t)$ for the SDKI model with $h=0.2$ starting from a qMPS with the parameters $(K_x, K_y, K_z)=(0.30, 0.50, 1.25)$ explored elsewhere[25], showing theoretical results (left side, $r<0$) and experimental results (right, $r>0$). The correlators exhibit two characteristic features of generic dual-unitary circuit dynamics: correlations spread with the maximum velocity along the 'light cones' of the circuit and correlations decay exponentially along the light cones. Note that the data in this plot are aggregated into bins ($r\in\{2j, 2j+1\}$ for $j>0$) containing symmetry-equivalent sites to smooth and reduce statistical fluctuations. **b**, The same correlator for a perturbed version of the SDKI model, which is not dual unitary. **c**,**d**, Traces of $C^{xx}(r,t)$, with data offset vertically by $0.1t$ for clarity, with dots showing the dual-unitary (**c**) and non-dual-unitary (**d**) experimental data. The error bars show the standard error due to finite sampling, and the coloured lines show the theoretical results. **e**, Log-linear plot of correlations along three different dual-unitary light-cone trajectories (the precise set of r and t values for each curve are indicated in the inset), with different offsets, $k=0, 1, 2$, from the centre of the light cone. Each dataset shows the characteristic exponential decay of correlations along the light cone.

The mid-circuit measurement and reset operations that enable holographic algorithms are performed with high fidelity by temporarily separating[28,29] the targeted and spectator ions from one another by a distance that is large ($\gtrsim$180 μm) compared with the $1/e^2$ radius of the resonant laser beam (between 13 and 20 μm depending on the zone) used for measurement and reset[30]. Crosstalk is further suppressed by temporarily moving the spectator ions off the radio-frequency null, which Doppler shifts the light from resonance[31], resulting in crosstalk errors on spectator qubits of $\lesssim 1\times10^{-3}$ for resets and $\lesssim 5\times10^{-3}$ for measurements in the worst case (that is, for a spectator qubit in the worst-possible location), and nearly an order of magnitude lower than that on average.

We prepare an initial qMPS corresponding to equation (4) with $W=\exp[-i\sum_{\alpha=x,y,z}K_\alpha\sigma^\alpha\otimes\sigma^\alpha]$. Using the circuit identities shown in Fig. 1c, we can implement tensors $\mathcal{N}$ (corresponding to W) as a unitary circuit by creating a Bell pair of the physical qubits to appropriately reorder the qubit lines. We ran nine holoQUADS time-evolution circuits (one for each duration $t=0, 1, \ldots, 8$ of time evolution), in each case executing 16 'slices' of holoQUADS (Fig. 1), resulting in a simulation of a 32-site section of the half-infinite MPS. The resource requirements for these circuits, such as the number of two-qubit gates used, are summarized in Table 1. Each circuit was repeated 1,000 times to reconstruct the estimates of correlation function $C^{xx}(r,t)$. The experimental results are summarized in Fig. 3, and show excellent quantitative agreement with the exact theoretical results in the thermodynamic limit (Fig. 3c, lines), which were obtained by contracting tensor-network diagrams described elsewhere[25] using the ITensor library[32]. We clearly observe that correlations propagate with the maximum velocity along a sharp light cone (Fig. 3a), which is the hallmark of dual-unitary circuit dynamics[33]; furthermore, correlations decay exponentially along the light cone, indicating the ergodic (non-integrable) character of the dynamics (Fig. 3e). Note that the data shown in Fig. 3 are only a slightly processed form of the raw experimental data. The only form of error mitigation we apply is to detect the leakage of the bond qubit out of the qubit-state manifold at the end of the holoQUADS algorithm (Supplementary Information). The results are post-selected on experimental trials without bond-qubit leakage, which amounts to neglecting less than 3% of the total data (Table 1 provides the leakage statistics).

Finally, we note that holoQUADS is not restricted to the simulation of dual-unitary models. Results from a holoQUADS

experiment on the Quantinuum H1-2 device for a non-dual-unitary model (a perturbed version of the SDKI model with the two-qubit gate $U = (u_+ \otimes u_-)e^{-i\frac{\pi}{4}\alpha(\sigma^x\otimes\sigma^x+\sigma^y\otimes\sigma^y)}(v_- \otimes v_+)$ for $\alpha = 1/2$), which agree well with theoretical predictions (determined by MPS numerics), are shown in Fig. 3b,d (Supplementary Information).

Discussion. Our results showcase both viability of quantum computers (for solving classically hard and practically relevant models of many-body quantum dynamics) and the benefits of mid-circuit measurement and qubit reuse (for simulating complex quantum dynamics of large, highly correlated quantum systems using quantum processors with limited qubit numbers). We emphasize that although we have demonstrated the holoQUADS algorithm for a finely tuned dual-unitary circuit, we have done so for benchmarking purposes. Dual-unitary circuits admit a convenient classical shortcut to a solution despite worst-case (from a classical simulation perspective) ballistic growth of entanglement, as well as retaining many of the features expected of generic quantum dynamics. Our implementation of holoQUADS does not take advantage of any of the fine-tuned self-dual structure of these circuits, and can be implemented to achieve significant resource savings in any situation where one would like to time evolve a correlated but not maximally entangled initial state, which we demonstrated with a holoQUADS experiment on a non-dual-unitary circuit.

Although our current results can be readily simulated by classical time-evolved block decimation methods (or by directly simulating the quantum algorithm, which involved no more than 11 qubits in this work), the excellent agreement with the exact results at all the simulation times demonstrates that we are currently limited by our qubit numbers rather than our gate fidelities. As quantum hardware with comparable gate fidelities and larger qubit numbers becomes available, which will enable deeper time evolutions of large systems, we expect that quantum tensor-network methods will enable further progress towards the ultimate goal of outperforming classical simulation capabilities on problems of direct physical relevance. Obvious targets for quantum advantage dynamics simulation include long-time dynamics of 1D systems for which the cost of classical time-evolved block decimation methods grows exponentially in time due to linear-in-time entanglement growth (Supplementary Information provides a resource estimate of a 1D dynamics quantum advantage experiment), the dynamics of two- and three-dimensional systems, which can be holographically represented as isometric tensor networks[34], or the dynamics of systems with longer-range (for example, truncated Coulomb) interactions.

Online content

Any methods, additional references, Nature Research reporting summaries, source data, extended data, supplementary information, acknowledgements, peer review information; details of author contributions and competing interests; and statements of data and code availability are available at https://doi.org/10.1038/s41567-022-01689-7.

Received: 8 September 2021; Accepted: 24 June 2022;
Published online: 4 August 2022

References

1. D'Alessio, L., Kafri, Y., Polkovnikov, A. & Rigol, M. From quantum chaos and eigenstate thermalization to statistical mechanics and thermodynamics. *Adv. Phys.* **65**, 239–362 (2016).
2. Abanin, D. A., Altman, E., Bloch, I. & Serbyn, M. Colloquium: many-body localization, thermalization, and entanglement. *Rev. Mod. Phys.* **91**, 021001 (2019).
3. Lloyd, S. Universal quantum simulators. *Science* **273**, 1073–1078 (1996).
4. Childs, A. M., Maslov, D., Nam, Y., Ross, N. J. & Su, Y. Toward the first quantum simulation with quantum speedup. *Proc. Natl. Acad. Sci. USA* **115**, 9456–9461 (2018).
5. Gross, C. & Bloch, I. Quantum simulations with ultracold atoms in optical lattices. *Science* **357**, 995–1001 (2017).
6. Monroe, C. et al. Programmable quantum simulations of spin systems with trapped ions. *Rev. Mod. Phys.* **93**, 025001 (2021).
7. Browaeys, A. & Lahaye, T. Many-body physics with individually controlled Rydberg atoms. *Nat. Phys.* **16**, 132–142 (2020).
8. Kim, I. H. Holographic quantum simulation. Preprint at https://arxiv.org/abs/1702.02093 (2017).
9. Kim, I. H. and Swingle, B. Robust entanglement renormalization on a noisy quantum computer. Preprint at https://arxiv.org/abs/1711.07500 (2017)
10. Foss-Feig, M. et al. Holographic quantum algorithms for simulating correlated spin systems. *Phys. Rev. Research* **3**, 033002 (2021).
11. Liu, J.-G., Zhang, Y.-H., Wan, Y. and Wang, L. Variational quantum eigensolver with fewer qubits. *Phys. Rev. Res.* **1,** 023025 https://journals.aps.org/prresearch/abstract/10.1103/PhysRevResearch.1.023025 (2019).
12. Barratt, F. et al. Parallel quantum simulation of large systems on small quantum computers. *NPJ Quantum Inf.* **7**, 79 https://www.nature.com/articles/s41534-021-00420-3 (2020).
13. Lin, Sheng-Hsuan, Dilip, R., Green, A. G., Smith, A. & Pollmann, F. Real- and imaginary-time evolution with compressed quantum circuits. *PRX Quantum* **2**, 010342 (2021).
14. Smith, A., Jobst, B., Green, A. G. and Pollmann, F. Crossing a topological phase transition with a quantum computer. *Phys. Rev. Res.* **4**, L022020 https://journals.aps.org/prresearch/abstract/10.1103/PhysRevResearch.4.L022020 (2019).
15. Yuan, X., Sun, J., Liu, J., Zhao, Q. and Zhou, Y. Quantum simulation with hybrid tensor networks. *Phys. Rev. Lett.* **127**, 04051 https://journals.aps.org/prl/abstract/10.1103/PhysRevLett.127.040501 (2020).
16. Eddins, A. et al. Doubling the size of quantum simulators by entanglement forging. *PRX Quantum* **3**, 010309 https://journals.aps.org/prxquantum/abstract/10.1103/PRXQuantum.3.010309 (2021).
17. Bravo-Prieto, C., Lumbreras-Zarapico, J., Tagliacozzo, L. & Latorre, JoséI. Scaling of variational quantum circuit depth for condensed matter systems. *Quantum* **4**, 272 (2020).
18. Calabrese, P. & Cardy, J. Evolution of entanglement entropy in one-dimensional systems. *J. Stat. Mech.* **2005**, P04010 (2005).
19. Schön, C., Solano, E., Verstraete, F., Cirac, J. I. & Wolf, M. M. Sequential generation of entangled multiqubit states. *Phys. Rev. Lett.* **95**, 110503 (2005).
20. Huggins, W., Patil, P., Mitchell, B., Whaley, K. B. & Stoudenmire, E. M. Towards quantum machine learning with tensor networks. *Quantum Sci. Technol.* **4**, 024001 (2019).
21. Akila, M., Gutkin, B. & Guhr, T. Particle-time duality in the kicked Ising spin chain. *J. Phys. A: Math. Theor.* **49**, 375101 (2016).
22. Bertini, B., Kos, P. & Prosen, T. Exact spectral form factor in a minimal model of many-body quantum chaos. *Phys. Rev. Lett.* **121**, 264101 (2018).
23. Bertini, B., Kos, P. & Prosen, T. Exact correlation functions for dual-unitary lattice models in 1+1 dimensions. *Phys. Rev. Lett.* **123**, 210601 (2019).
24. Gopalakrishnan, S. & Lamacraft, A. Unitary circuits of finite depth and infinite width from quantum channels. *Phys. Rev. B* **100**, 064309 (2019).
25. Piroli, L., Bertini, B., Cirac, J. I. & Prosen, T. Exact dynamics in dual-unitary quantum circuits. *Phys. Rev. B* **101**, 094304 (2020).
26. Bertini, B., Kos, P. & Prosen, T. Operator entanglement in local quantum circuits I: chaotic dual-unitary circuits. *SciPost Phys.* **8**, 067 (2020).
27. Claeys, P. W. & Lamacraft, A. Ergodic and nonergodic dual-unitary quantum circuits with arbitrary local Hilbert space dimension. *Phys. Rev. Lett.* **126**, 100603 (2021).
28. Barrett, M. D. et al. Deterministic quantum teleportation of atomic qubits. *Nature* **429**, 737–739 (2004).
29. Chiaverini, J. et al. Realization of quantum error correction. *Nature* **432**, 602–605 (2004).
30. Olmschenk, S. et al. Manipulation and detection of a trapped Yb^+ hyperfine qubit. *Phys. Rev. A* **76**, 052314 (2007).
31. Berkeland, D. J., Miller, J. D., Bergquist, J. C., Itano, W. M. & Wineland, D. J. Minimization of ion micromotion in a Paul trap. *J. Appl. Phys.* **83**, 5025–5033 (1998).
32. Fishman, M., White, S. R. and Stoudenmire, E. M. The ITensor software library for tensor network calculations. Preprint at https://arxiv.org/abs/2007.14822 (2020).
33. Claeys, P. W. & Lamacraft, A. Maximum velocity quantum circuits. *Phys. Rev. Research* **2**, 033032 (2020).
34. Zaletel, M. P. & Pollmann, F. Isometric tensor network states in two dimensions. *Phys. Rev. Lett.* **124**, 037201 (2020).
35. Pino, J. M. et al. Demonstration of the trapped-ion quantum CCD computer architecture. *Nature* **592**, 209–213 (2021).
36. Palmero, M., Bowler, R., Gaebler, J. P., Leibfried, D. & Muga, J. G. Fast transport of mixed-species ion chains within a Paul trap. *Phys. Rev. A* **90**, 053408 (2014).

37. Home, J. P. & Steane, A. M. Electrode configurations for fast separation of trapped ions. *Quantum Inf. Comput.* **6**, 289–325 (2006).
38. Splatt, F. et al. Deterministic reordering of $^{40}Ca^{+}$ ions in a linear segmented Paul trap. *New J. Phys.* **11**, 103008 (2009).
39. Bezanson, J., Edelman, A., Karpinski, S. & Shah, V. B. Julia: a fresh approach to numerical computing. *SIAM Rev.* **59**, 65–98 (2017).
40. Abraham, H. et al. Qiskit: an open-source framework for quantum computing. *Zenodo* https://zenodo.org/record/2562111 (2019).

Data availability

The raw data produced by the Quantinuum devices for this work are available in Supplementary Data 1.

Code availability

The code used to generate data for this work is available from the corresponding author upon reasonable request.

Acknowledgements

This work was made possible by a large group of people, and the authors would like to thank the entire Quantinuum team for their many contributions. The experiments reported in this manuscript were performed on Quantinuum's H1-1 and H1-2 system models, which are powered by Honeywell ion traps. We thank C. Baldwin for helpful discussions regarding the performance benchmarks on H1-1 and H1-2. We used the ITensor library[32], written in Julia[39], to perform the tensor-network contractions to generate the theory curves. Quantum circuits were prepared and simulated using the Qiskit library created by IBM[40]. A.C.P. was supported by NSF Convergence Accelerator Track C award 2040549.

Author contributions

E.C., M.F.-F. and A.C.P. conceived the experiment. J.B., D.F., J.G., D.G., A.H., K.L., B.N. and R.S. executed the experiment on the Quantinuum quantum computer. E.C. performed the theoretical analysis and numerical simulations. E.C., M.F.-F. and A.C.P. analysed the experimental data. M.F.-F. and D.H. coordinated and supervised the project. E.C., M.F.-F., A.C.P. and D.H. wrote the manuscript and the Supplementary Information. All the authors edited the manuscript.

Competing interests

The authors declare no competing interests.

Additional information

Supplementary information The online version contains supplementary material available at https://doi.org/10.1038/s41567-022-01689-7.

Correspondence and requests for materials should be addressed to Eli Chertkov.

Peer review information *Nature Physics* thanks Luca Tagliacozzo and the other, anonymous, reviewer(s) for their contribution to the peer review of this work.

Reprints and permissions information is available at www.nature.com/reprints.